

# Modelling Improper Complex-Valued Signals using a Stochastic Differential Equation Approach

Adam M. Sykulski<sup>1</sup>, Sofia C. Olhede<sup>2</sup> and Hanna M. Sykulska-Lawrence<sup>3</sup>

## Abstract

Complex-valued signals are often observed to be improper, meaning that the complementary covariance or complementary spectrum of the signal is non-zero. Stochastic models for improper signals are often represented as widely linear filters of discrete-time noise processes. In this paper we propose an alternative perspective and model the signal in continuous time using a stochastic differential equation (SDE) approach. Specifically, we propose a first order SDE representation of a complex-valued signal which generates impropriety in the form of elliptical oscillations in the signal's trajectory. The key benefit of our approach is that elliptical trajectories can be generated using one simple first order SDE, whereas the alternative of bivariate modelling requires more complicated vectorised or higher order SDE representations. The second key benefit is that parameter estimation can be performed directly using only the power spectral density of the complex-valued signal, without having to compute cross spectra of individual signal components. Our proposed model can be interpreted as a widely linear version of the complex Ornstein-Uhlenbeck (OU) process. We determine properties of the model including the conditions for stationarity, and the geometrical structure of the elliptical oscillations. We apply the model to measure periodic and elliptical properties of Earth's polar motion.

**Keywords:** Improper; Widely Linear; Ornstein-Uhlenbeck; Whittle Likelihood; Polar Motion

## 1 Introduction

The signal processing community has given considerable attention to the modelling of improper complex-valued signals; see, e.g. Yoon and Leib (1997); Schreier and Scharf (2003); Jelfs et al. (2012); Sykulski et al. (2017). The motivation for using such approaches is that by modelling the complementary covariance (as well as the covariance) such models capture *noncircularity* in the second-order structure of stationary complex-valued signals (Schreier and Scharf, 2010). A type of noncircularity of particular interest is that of *elliptical oscillations* in a signal's trajectory, which are observed across numerous applications including oceanography (Lilly and Gascard, 2006), seismology (Sykulski et al., 2016a), and planetary geophysics (Barkin and Ferrandiz, 2010).

Thus far, the literature on stochastic modelling of improper signals has primarily focused on widely linear filters of discrete-time noise models, see e.g. Picinbono and Chevalier (1995); Navarro-Moreno (2008); Sykulski et al. (2016a). In many physical applications however, it is preferable to model the evolution of a signal in continuous time using stochastic differential equations (SDEs), because this allows explicit con-

<sup>1</sup> Department of Mathematics and Statistics, Lancaster University, UK (email: a.sykulski@lancaster.ac.uk)

<sup>2</sup> École polytechnique fédérale de Lausanne, Switzerland

<sup>3</sup> Department of Aeronautical and Astronautical Engineering, University of Southampton, UK

nections to be made with underlying dynamical equations, such that parameters are more physically interpretable (see e.g. Brown and Crane (1969); Arató et al. (1962); Veneziani et al. (2004)).

In this paper we propose a novel approach of applying a widely linear representation to a first-order SDE. We demonstrate that this creates elliptical oscillations in the signal’s trajectory. This approach is complementary to, but distinct from, the approach of Oya et al. (2011) which uses Karhunen-Loève expansions to generate improper continuous-time nonstationary signals. We show how our first order SDE, shown in (1), can be considered as a widely linear generalisation of the complex Ornstein-Uhlenbeck (OU) process (Arató et al., 1962; Sykulski et al., 2016b), which maps out circular oscillations in a signal’s trajectory.

We will give focus to the widely linear dynamics of our specifying SDE in (1). This equation specifies the geometry of the signal dynamics, commonly studied by using *time delay embedding plots*, see e.g. Kantz and Schreiber (2004). We shall show that the time delay embedding plots map out an ellipse, as has been observed in Lilly and Olhede (2009); Lilly and Gascard (2006); Schreier (2008), but in contrast to the aforementioned literature we are able to directly interpret the dynamics in terms of the SDE. Understanding of dynamics requires a continuous-time model, rather than a discrete-time specification.

There are three novel contributions of this paper: 1) Proposing an SDE model for complex-valued signals that creates elliptical oscillations using a parsimonious and simple first order model, i.e. we do not require higher derivatives or vectorised representations to create elliptical curvature. 2) Deriving properties of our model including conditions for stationarity, the analytical form of the power spectral density, and the geometrical relationship between the SDE parameters and the properties of the elliptical oscillations (e.g. the eccentricity and orientation). 3) Providing computationally efficient and practical techniques for fitting our model to real signals. Specifically, we show that the model can be fitted to observed signals by performing parameter estimation in the frequency domain using only the theoretical and observed power spectral density. We do not have to compute individual and cross spectra of the signal components, as would be required in a bivariate analysis. Finally, we demonstrate the applicability of our model by studying the oscillations contained within Earth’s polar motion.

## 2 A Widely Linear First Order SDE

We propose a complex-valued continuous-time signal given by  $z(t) = x(t) + iy(t)$ , where  $i \equiv \sqrt{-1}$  and the evolution of  $z(t)$  is defined by the following first order SDE

$$dz(t) = (-\alpha_1 + i\beta_1)z(t)dt + (-\alpha_2 + i\beta_2)z^*(t)dt + dW(t), \quad (1)$$

where  $z^*(t)$  is the complex conjugate of  $z(t)$ . The parameters  $\{\alpha_1, \beta_1, \alpha_2, \beta_2\}$  are real-valued, and we place constraints on these parameters which ensure  $z(t)$  is stationary in Section 2.2.  $W(t)$  is a Wiener process, whose increments follow a complex normal distribution such that  $B = \{W(t + \delta) - W(t)\}/\sqrt{\delta} \sim \mathcal{CN}(0, \sigma^2, r)$ , where  $\sigma^2 = E(BB^*)$  defines the variance of the complex normal, and  $r = E\{B^2\}$  defines the *pseudo*-variance and is a complex-valued quantity in general (Schreier and Scharf, 2010).

If we set  $\alpha_2 = \beta_2 = r = 0$  in (1) then we recover the regular complex OU process of Arató et al. (1962) which is a *proper* process meaning that the complementary covariance defined by  $r_z(\tau) = E\{z(t)z(t + \tau)\}$  is zero for all  $\tau$ . In general however, (1) is improper (as we shall prove in this section) such that  $r_z(\tau)$  is non-zero for some values of  $\tau$ . Therefore (1) specifies genuine complex dynamics in a signal using a stochastic differential equation approach. The inclusion of the  $z^*(t)$  term in (1) can be interpreted as a widely linear representation of the SDE—note that analogous representations for discrete-time autoregressive signals have been made in Navarro-Moreno (2008); Sykulski et al. (2016a). The noise term  $dW(t)$  is itself improper and can also be given a widely linear representation (Picinbono and Bondon, 1997).

As a result, we shall henceforth refer to (1) as the *widely linear* complex OU process—as it generalises the complex OU process of Arató et al. (1962) with the addition of the  $z^*(t)$  term and by allowing for improper noise increments  $dW(t)$ .

## 2.1 Process Realisations

In Fig. 1 we show two realisations of the widely linear complex OU process under two different sets of parameter values, along with their empirical power spectral densities. The signals are generated using the Euler-Maruyama scheme. In each panel we overlay the theoretical power spectral density whose functional form will be derived in Section 2.3. As can be seen from the figure, the process generates elliptical oscillations in the signal trajectory from a first order model. These elliptical oscillations are seen to have differing eccentricities, orientations, and rates of damping in each example. These oscillations create two peaks in the power spectral density, located at the same corresponding negative and positive frequency.

Equation (1) specifies the evolution or dynamics of  $z(t)$ . If we try to predict  $z(t + \delta t)$  given  $z(t)$ , then as  $dW(t)$  is not predictable, we have that

$$z(t + \delta t) - z(t) = \int_t^{t+\delta t} \{(-\alpha_1 + i\beta_1)z(t')dt' + (-\alpha_2 + i\beta_2)z^*(t')dt' + dW(t')\}. \quad (2)$$

We see directly from this equation that the increment is a widely linear transformation of  $z(t)$ . Starting from the notion of complex geometry (Lindell, 1992, Ch. 1), we can describe the linear vector space mapped out by complex vectors. In this space the notion of a line has been replaced by an ellipse. This ellipse can collapse to a line or a circle under special circumstances, if perturbed by  $dW(t')$ . The complex vector in (2) maps out a trajectory in the plane  $(x, y)$  where  $z(t) = x(t) + iy(t)$ .

Thus at every time point  $t'$ , a modification is formed by adding an ellipse to the current position  $z(t)$  to get to  $z(t + \delta t)$ . And as  $z(t)$  is fixed, if we view the process conditionally on its starting point, then (2) maps out a sequence of superimposed ellipses. To understand the geometry of this ellipse we consider a deterministic version of (1) and (2) where  $dW(t) = 0$ . Expressing this in terms of  $x(t)$  and  $y(t)$  we have that

$$dx(t) + idy(t) = \{-(\alpha_1 + \alpha_2)x(t) + (\beta_2 - \beta_1)y(t)\} dt + i\{(\beta_1 + \beta_2)x(t) + (\alpha_2 - \alpha_1)y(t)\} dt, \quad (3)$$

such that the parameter  $\alpha_1$  sets the damping of the process in both  $x(t)$  and  $y(t)$  if it is greater than zero—as is the case with regular real-valued OU processes. The parameters  $\{\alpha_2, \beta_1, \beta_2\}$  set the geometry of the ellipse of the deterministic motion as they cause asymmetric interactions between  $x(t)$  and  $y(t)$ . As discussed already, the ellipse becomes a circle if  $\alpha_2 = \beta_2 = 0$ , and this can be clearly seen from (3) when the damping  $\alpha_1$  is set to zero. The other extreme is when the ellipse becomes a line which occurs when  $\beta_1^2 = \alpha_2^2 + \beta_2^2$ . To show this is the case, consider (3) and set this equal to zero when  $x(t) = Cy(t)$  (where  $C$  is some constant), and set the damping  $\alpha_1 = 0$ . From (3) we then solve for the simultaneous equations  $-\alpha_2 = C(\beta_2 - \beta_1)$  and  $\beta_1 + \beta_2 = C\alpha_2$  which yields  $\beta_1^2 = \alpha_2^2 + \beta_2^2$  for the special case of linear motion. These special cases will be verified in Section 2.2 where we formally derive the eccentricity of the elliptical oscillations of the stochastic process of (1).

This geometric structure can be related to time delay embedding plots (Kantz and Schreiber, 2004). In an embedding plot,  $\Re\{z(t)\}$  would be plotted against  $\Im\{z(t)\}$  across time, and this will capture the dynamics of the sde as encapsulated by the ellipse geometry. Finally, note that (2) is a continuous time specification. It demonstrates that increments in the process  $z(t)$  associated with arbitrary increments  $\delta t$  are arrived at by a widely linear operation with some noisy offset. Equation (2) also shows that  $z(t)$  will trace out a continuous time trajectory in the plane, as specified by  $(x(t), y(t))$ .

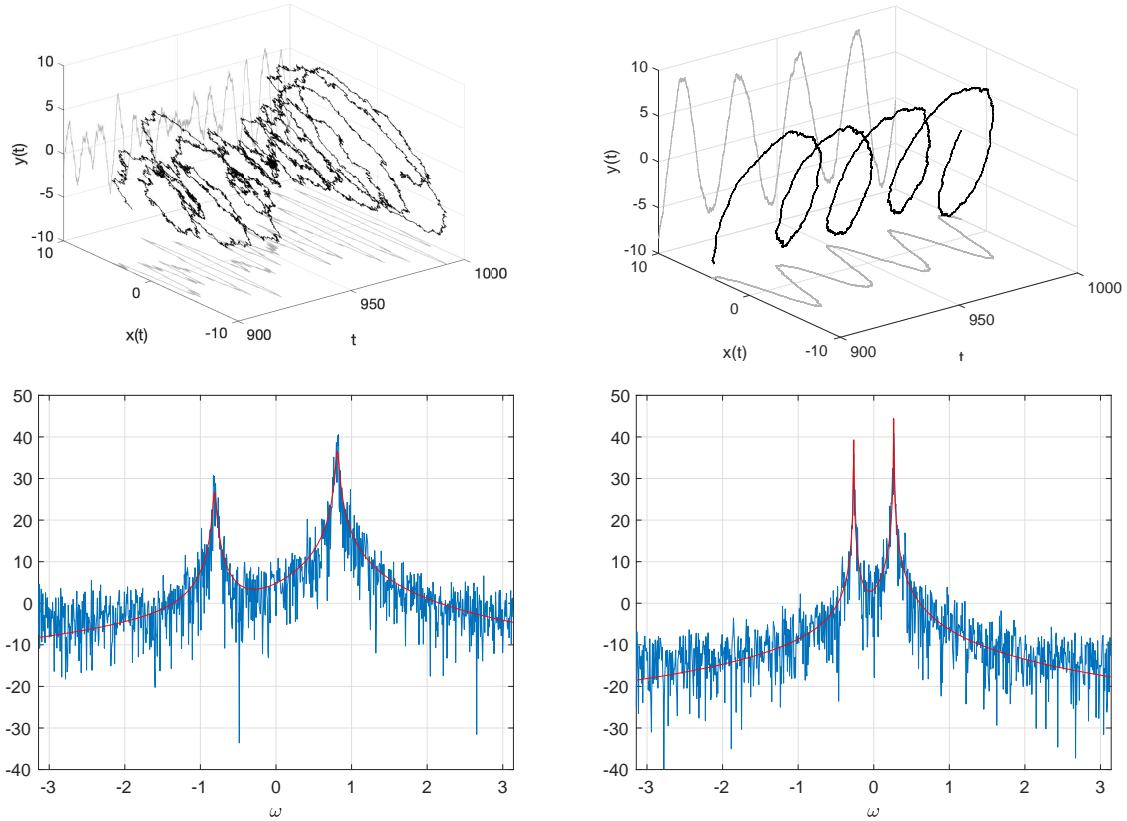


Figure 1: The top row displays two realisations of the widely linear complex OU process  $z(t) = x(t) + iy(t)$  of (1) with parameters  $\{\alpha_1 = 0.2, \beta_1 = 1, \alpha_2 = -0.5, \beta_2 = -0.3, \sigma^2 = 2, r = 0.6 + i\}$  (left) and  $\{\alpha_1 = 0.02, \beta_1 = 0.5, \alpha_2 = 0.3, \beta_2 = 0.3, \sigma^2 = 0.15, r = -0.09 - 0.09i\}$  (right) generated using the Euler-Maruyama scheme. We plot  $z(t)$  in black, and the  $x(t)$  and  $y(t)$  components in grayscale in the 3-D plot. We simulate from  $t = 0$  to  $t = 1000$  and plot both signals from  $t = 900$  to  $t = 1000$  only. In the bottom row we display the empirical periodograms of the full signals subsampled at integer values of  $t$  (plotted on a decibel scale), and we overlay the theoretical power spectral from (11) in red. The slight discrepancy at high positive and negative frequencies is due to aliasing effects on the periodogram.

## 2.2 Process Properties

To further understand the properties of (1), we define a *circular* real-valued bivariate OU process (see also Veneziani et al. (2004)) given by

$$\begin{bmatrix} d\tilde{x}(t) \\ d\tilde{y}(t) \end{bmatrix} = \begin{bmatrix} -\alpha & -\beta \\ \beta & -\alpha \end{bmatrix} \begin{bmatrix} \tilde{x}(t) \\ \tilde{y}(t) \end{bmatrix} dt + \frac{A}{\sqrt{2}} \begin{bmatrix} dW_1(t) \\ dW_2(t) \end{bmatrix}, \quad (4)$$

where  $\alpha > 0$  ensures stationarity,  $\beta \in \mathbb{R}$  sets the frequency of the circular oscillation, and  $dW_1(t)$  and  $dW_2(t)$  are independent real-valued Wiener process increments such that  $\{W_1(t + \delta) - W_1(t)\}/\sqrt{\delta} \sim \mathcal{N}(0, 1)$  and  $\{W_2(t + \delta) - W_2(t)\}/\sqrt{\delta} \sim \mathcal{N}(0, 1)$ . We refer the reader to Vatiwutipong and Phewchean (2019) for a more general overview of multivariate OU processes. Setting  $\tilde{z}(t) = \tilde{x}(t) + i\tilde{y}(t)$  recovers the complex OU process of Arató et al. (1962). In other words, (1) and (4) are equivalent when  $\alpha_1 = \alpha$ ,  $\beta_1 = \beta$ ,  $\sigma^2 = A^2$ , and  $\alpha_2 = \beta_2 = r = 0$ .

We now transform (4) to create elliptical oscillations by defining a new process

$$\begin{bmatrix} x(t) \\ y(t) \end{bmatrix} = QP \begin{bmatrix} \tilde{x}(t) \\ \tilde{y}(t) \end{bmatrix}, \quad Q = \begin{bmatrix} \cos \psi & -\sin \psi \\ \sin \psi & \cos \psi \end{bmatrix}, \quad P = \begin{bmatrix} \frac{1}{\rho} & 0 \\ 0 & \rho \end{bmatrix}. \quad (5)$$

The parameter  $\rho$  is a stretching parameter, and  $\psi$  is a rotation parameter, which respectively set the eccentricity and orientation of the elliptical oscillations. For uniqueness we restrict  $0 < \rho \leq 1$  and  $-\pi/2 \leq \psi \leq \pi/2$ . Note that  $P$  must be applied first in (5) for  $Q$  to have an effect. We can interpret (5) as a physical deformation of the circular process of (4).

We now express  $[x(t) \ y(t)]^T$  as a self-contained bivariate SDE by combining (4) and (5) such that

$$\begin{bmatrix} dx(t) \\ dy(t) \end{bmatrix} = QP \left\{ \Omega P^{-1} Q^T \begin{bmatrix} x(t) \\ y(t) \end{bmatrix} dt + \frac{A}{\sqrt{2}} \begin{bmatrix} dW_1(t) \\ dW_2(t) \end{bmatrix} \right\}, \quad (6)$$

where we use that  $Q^{-1} = Q^T$  and where we define

$$\Omega = \begin{bmatrix} -\alpha & -\beta \\ \beta & -\alpha \end{bmatrix}.$$

Equation (6) is a complicated vectorised expression for generating elliptical oscillations, which we contrast with the simpler expression given in (1) using the complex representation. However, (6) is useful for understanding the dynamics of, and placing parameter constraints on, equation (1), as we shall now show. Specifically, we set  $z(t) = x(t) + iy(t)$  and show that (6) can then be written in the form of (1). To do this we define the relationship

$$\begin{bmatrix} x(t) \\ y(t) \end{bmatrix} = \frac{1}{2} T \begin{bmatrix} z(t) \\ z^*(t) \end{bmatrix}, \quad T = \begin{bmatrix} 1 & 1 \\ -i & i \end{bmatrix}. \quad (7)$$

By combining (6) and (7) we then obtain

$$\begin{bmatrix} dz(t) \\ dz^*(t) \end{bmatrix} = \frac{1}{2} T^H L T \begin{bmatrix} z(t) \\ z^*(t) \end{bmatrix} dt + T^H Q P \frac{A}{\sqrt{2}} \begin{bmatrix} dW_1(t) \\ dW_2(t) \end{bmatrix}, \quad (8)$$

where  $L = QP\Omega P^{-1}Q^T$ . The widely linear complex OU SDE is then obtained from expanding (8) and taking the top row, such that we obtain

$$dz(t) = \left( -\alpha + i\frac{\beta}{2} \left\{ \frac{1}{\rho^2} + \rho^2 \right\} \right) z(t) dt + \frac{\beta}{2} \left\{ \frac{1}{\rho^2} - \rho^2 \right\} (\sin 2\psi - i \cos 2\psi) z^*(t) dt + dW(t), \quad (9)$$

Table 1: This table provides a mapping between the parameters of the widely linear complex OU (1) and the bivariate process of (6). The function  $\text{atan2}$  is the four quadrant inverse tangent and  $\text{sgn}$  is the signum function.

Bivariate SDE to Complex SDE	Complex SDE to Bivariate SDE
$\alpha_1 = \alpha$	$\alpha = \alpha_1$
$\beta_1 = \frac{\beta}{2} \left( \rho^2 + \frac{1}{\rho^2} \right)$	$\beta = \text{sgn}(\beta_1) \sqrt{\beta_1^2 - \alpha_2^2 - \beta_2^2}$
$\alpha_2 = \frac{\beta}{2} \left( \rho^2 - \frac{1}{\rho^2} \right) \sin 2\psi$	$\rho = \left( \frac{ \beta_1  - \sqrt{\alpha_2^2 + \beta_2^2}}{ \beta_1  + \sqrt{\alpha_2^2 + \beta_2^2}} \right)^{1/4}$
$\beta_2 = \frac{\beta}{2} \left( \rho^2 - \frac{1}{\rho^2} \right) \cos 2\psi$	$\psi = \frac{\text{sgn}(-\beta_1)}{2} \text{atan2}(\alpha_2, \text{sgn}(-\beta_1)\beta_2)$
$\sigma^2 = \frac{A^2}{2} \left( \rho^2 + \frac{1}{\rho^2} \right)$	$A^2 = \sigma^2 \frac{\sqrt{\beta_1^2 - \alpha_2^2 - \beta_2^2}}{ \beta_1 }$

where the increment process  $dW(t)$  is defined by

$$\sigma^2 = \frac{A^2}{2} \left( \frac{1}{\rho^2} + \rho^2 \right), \quad r = \frac{A^2}{2} \left( \frac{1}{\rho^2} - \rho^2 \right) e^{i2\psi}.$$

By equating the parameters in (1) and (9) we can obtain an exact one-to-one mapping between the parameter set  $\{\alpha_1, \beta_1, \alpha_2, \beta_2, \sigma^2\}$  of the widely linear complex SDE of (1), and the parameter set  $\{\alpha, \beta, \rho, \psi, A^2\}$  of the bivariate SDE of (6). The mapping in each direction is given in Table 1. The parameter  $r$ , which sets the pseudo-variance of the complex-valued increment process  $dW(t)$ , is redundant and should be set as

$$r = -\frac{\sigma^2}{\beta_1}(\beta_2 + i\alpha_2),$$

such that the widely linear complex OU is reduced to five free parameters from mapping to an elliptically transformed bivariate OU process. Setting  $\rho = 1$  in (9) (and Table 1) recovers the regular three-parameter complex OU process of Arató et al. (1962) and (4).

In the widely linear setting, we observe from Table 1 the simple relationship that  $\alpha_1 = \alpha$ , meaning  $\alpha_1$  sets the damping rate of the oscillations in (1), and we thus require  $\alpha_1 > 0$  for the widely linear complex OU to be stationary. The parameters  $\{\beta_1, \alpha_2, \beta_2\}$  jointly determine  $\{\beta, \rho, \psi\}$  (the oscillation frequency, eccentricity and orientation) and we require  $|\beta_1| > \sqrt{\alpha_2^2 + \beta_2^2}$  to create a valid mapping between the two processes. The eccentricity of the oscillations is given by

$$\varepsilon = \sqrt{1 - \rho^4} = \sqrt{\frac{2\sqrt{\alpha_2^2 + \beta_2^2}}{|\beta_1| + \sqrt{\alpha_2^2 + \beta_2^2}}},$$

such that larger values of  $\alpha_2$  and  $\beta_2$  create more eccentric oscillations. This formally establishes the geometric properties of the elliptical oscillations and verifies the results from Section 2.1 that the oscillations are circular when  $\alpha_2 = \beta_2 = 0$ , and collapse to a line as  $\alpha_2^2 + \beta_2^2$  approaches  $\beta_1^2$ . In the next section we derive the power spectral density of the widely linear complex OU which will provide yet further intuition on the effect of the different parameters.

Overall, we see that complex-valued modelling provides a much more straightforward SDE representation of elliptical oscillations than bivariate modelling, as shown in (1) and Fig. 1. However, mapping to an underpinning bivariate process, as in (6), allows us to further understand the geometry and dynamics of the elliptical oscillations, as well as place necessary parameter constraints.

A similar mapping analysis was performed with discrete-time models in Sykulski et al. (2016a) by equating a widely linear autoregressive AR(1) process to a corresponding bivariate process. The mappings between the parameters are significantly different here as compared with those found in Sykulski et al. (2016a) for discrete time. There are two reasons why these mappings are so different. First, although an AR(1) process can generally be interpreted as a discrete-time analogue of an OU process, there is no simple transformation between their sets of parameters in the widely linear case, as we show in Appendix A. This is consistent with Brockwell (2001) who discusses the nontrivial relationship between sampled CARMA (continuous ARMA) models and regular discrete-time ARMA models. Secondly, the widely linear complex OU process of (1) has coefficients given in Cartesian form, whereas the coefficients of the widely linear AR(1) are given in polar form (see (16) in Appendix 5). These parameterizations in each case make sense as the mappings between the OU and AR processes are then straightforward in the regular (non widely linear) case, see (17)–(19) in Appendix A. However, these choices of parameterizations cause further departures in the parameter mappings in the widely linear case. As a result, the conditions for stationarity, and the geometrical properties of elliptical oscillations, are entirely different in the continuous-time complex OU proposed in this paper, and the discrete-time AR(1) proposed in Sykulski et al. (2016a).

### 2.3 The Power Spectral Density

For stationary complex-valued processes the power spectral density can in general be defined from the autocovariance sequence of the process, such that

$$S_z(\omega) = \int s_z(\tau) e^{-i\omega\tau} d\tau, \quad s_z(\tau) = E\{z(t)z^*(t+\tau)\}.$$

The power spectral density of the regular complex OU process of Arató et al. (1962) is given by Sykulski et al. (2016b)

$$S_z(\omega) = \frac{\sigma^2}{\alpha_1^2 + (\omega - \beta_2)^2} = \frac{A^2}{\alpha^2 + (\omega - \beta)^2}, \quad (10)$$

which we have provided both in terms of the parameterization of (1) (with  $\alpha_2 = \beta_2 = r = 0$ ), and of the circular bivariate process of (4). Note that despite being a proper process, the spectral density will contain energy at both negative and positive frequencies, decaying at rate  $\omega^{-2}$  from the peak frequency.

The power spectral density of the widely linear complex OU process is given by

$$S_z(\omega) = A^2 \left\{ \frac{\left(\frac{1}{\rho} + \rho\right)^2}{\alpha^2 + (\omega - \beta)^2} + \frac{\left(\frac{1}{\rho} - \rho\right)^2}{\alpha^2 + (\omega + \beta)^2} \right\}, \quad (11)$$

which is given in terms of the parameterization of the elliptical bivariate process of (5). Then to find the power spectral density in terms of (1) one simply substitutes using the transformations in the right column of Table 1. The derivation of (11) is provided in Appendix B.

Intuition is gained by examining (11). While (10) has just one peak in the spectral density located at  $\omega = \beta$ , (11) has two peaks located at  $\omega = \pm\beta$ . The rate of damping of both peaks is determined by  $\alpha$ , and the ratio of magnitudes of the two peaks is determined by  $\rho$ . Note that the orientation parameter  $\psi$  does

not feature in the power spectral density. When (11) is represented using the parameters of (1) then we see that  $\alpha_1$  defines the damping of the two peaks, and  $\{\beta_1, \alpha_2, \beta_2\}$  together determine the peak locations and their relative magnitudes. We have overlaid the power spectral density of (11) over the periodogram of the simulated series in Fig. 1.

To fully specify the properties of the widely linear complex OU process, we also need to derive the *complementary* spectrum defined by

$$R_z(\omega) = \int r_z(\tau) e^{-i\omega\tau} d\tau, \quad r_z(\tau) = E\{z(t)z(t+\tau)\}.$$

The regular complex OU process of Arató et al. (1962) is a proper process and therefore  $R_z(\omega) = r_z(\tau) = 0$ . The widely linear complex OU has a complementary spectrum given by

$$R_z(\omega) = \frac{A^2}{4} \left( \frac{1}{\rho^2} - \rho^2 \right) \left\{ \frac{1}{\alpha^2 + (\omega - \beta)^2} + \frac{1}{\alpha^2 + (\omega + \beta)^2} \right\} e^{i2\psi}, \quad (12)$$

which is dependent on  $\psi$ , as well as all the other parameters. We see that as long as  $\rho < 1$  then  $R_z(\omega)$  is non-zero such that  $r_z(\tau)$  is also non-zero and the widely linear complex OU is an improper process as intended. The derivation of (12) can also be found in Appendix B. We note that full specification of the power spectral density and complementary spectrum allows for an exact method of simulation based on circulant embedding and Fourier transforms, as an alternative to Euler-Maruyama, see Sykulski and Percival (2016) for details.

### 3 Parameter estimation

The widely linear Complex OU of (1) is an improper process, as we have shown. Therefore to estimate parameters using a maximum likelihood approach from an observed complex-valued signal, we would need to consider either the complementary covariance or the complementary spectrum (in addition to the autocovariance and power spectral density). Similarly, if we were to use a bivariate representation of the signal, then the cross-spectral density or cross covariance of the signal components must be considered in addition to the power spectral density or autocovariance of the individual signal components. Such methods are outlined in detail in Sykulski et al. (2017).

In this section we outline an alternative but practical *semi-parametric* pseudo-likelihood approach which is applicable to the complex SDE representation of (1). In particular, the method only requires computation of the observed power spectral density of the complex-valued signal, where the observed complementary spectrum is not needed to obtain parameter estimates. This is achieved by allowing the orientation parameter of the ellipse,  $\psi$ , to be estimated non-parametrically, as we now describe.

Specifically, consider a length- $n$  observed complex-valued signal  $\mathbf{Z} = [Z_1, \dots, Z_n]$  where the signal is regularly sampled at intervals denoted by  $\Delta$ . To obtain parameter estimates we maximise a pseudo-likelihood known as the Whittle likelihood which is given by

$$\ell_S(\boldsymbol{\theta}) = - \sum_{\omega \in \Omega} \left\{ \log S_z(\omega; \boldsymbol{\theta}) + \frac{I_Z(\omega)}{S_z(\omega; \boldsymbol{\theta})} \right\}, \quad (13)$$

where  $I_Z(\omega) = |J_Z(\omega)|^2$  is the periodogram and  $J_Z(\omega)$  is the Discrete Fourier Transform given by

$$J_Z(\omega) = \frac{\sqrt{\Delta}}{N} \sum_{t=1}^n Z_t e^{-i\omega t \Delta},$$

and  $\Omega$  is the set of Fourier frequencies given by

$$\Omega = \frac{2\pi}{n\Delta} (-\lceil n/2 \rceil + 1, \dots, -1, 0, 1, \dots, \lfloor n/2 \rfloor). \quad (14)$$

This approach can be adapted to irregularly spaced observations using the techniques described in Matsuda and Yajima (2009).

To fit the widely linear complex OU, we substitute (11) into (13) and maximise  $\ell_S(\boldsymbol{\theta})$  to find the parameter estimates. We note that this can only be done over the parameter vector  $\boldsymbol{\theta} = \{\alpha, \beta, \rho, A^2\}$  as  $\psi$  is not present in the power spectral density of (11). We therefore propose the following non-parametric estimate

$$\hat{\psi} = \frac{1}{2} \left[ \arg\{J(\hat{\beta})\} + \arg\{J(-\hat{\beta})\} \right], \quad (15)$$

where  $\hat{\beta}$  is the Whittle estimate of  $\beta$  from maximising (13). The parameter estimates corresponding to (1) are then found using the right column of Table 1.

Therefore our parameter estimation procedure can be performed semi-parametrically without having to compute the complementary spectrum. The reason for this is that the eccentricity of the ellipse is fully defined by the power spectral density, such that impropriety can be captured and estimated *without* having to consider the complementary spectrum. As a result, we found this method to be more robust to misspecified models, particularly when performing our analysis of polar motion signals, as we shortly describe. We also found the optimisation procedure to converge quickly and robustly when only having to jointly estimate four parameters parametrically, rather than five.

In the bivariate setting however, the described semi-parametric approach would still require computation of three spectra: the power spectral density of  $x$ , the power spectral density of  $y$ , and the cross-spectral density of  $x$  and  $y$ . This highlights the significant practical appeal of complex representations over bivariate: not only is the SDE representation more compact, but also estimation can be performed more flexibly by taking advantage of the rich information in the power spectral density of  $z$  (as demonstrated in Fig 1).

Another practical appeal of this approach is that the likelihood estimate can be made even more semi-parametric by only including a subset of frequencies from (14) in the Whittle fit of (13) (see also Robinson et al. (1995)). This can be useful when the periodogram is contaminated by high frequency noise (and high frequencies should hence be excluded from the fit), or the chosen model is known to only be correct in a narrow range of frequencies, perhaps because an aggregation of effects has been observed. Indeed we shall employ such procedures in Section 4 to separate the annual and Chandler wobble oscillations of Earth's polar motion.

Other modifications to Whittle likelihood including tapering and differencing the signal, or debiasing the estimates to account for aliasing and spectral blurring (see Sykulski et al. (2019) for a review). We did not find such modifications to be needed for the widely linear complex OU process. This is because the process has a relatively small dynamic range, owing to the  $\omega^{-2}$  decay in (11), such that there is only a small amount of spectral blurring present in the periodogram.

## 4 Earth's polar motion

Polar motion measures the deviation of Earth's rotational axis relative to its crust. In Fig. 2 we plot Earth's polar motion from 1845 to present day in orthogonal  $x$  and  $y$  directions, as measured in milliarcseconds (mas), where 100mas corresponds to a deviation of approximately 3 metres. This data is publicly available from the International Earth Rotation and Reference Systems Service Earth Orientation products<sup>4</sup>. We

<sup>4</sup>[www.iers.org/IERS/EN/DataProducts/EarthOrientationData/eop.html](http://www.iers.org/IERS/EN/DataProducts/EarthOrientationData/eop.html)

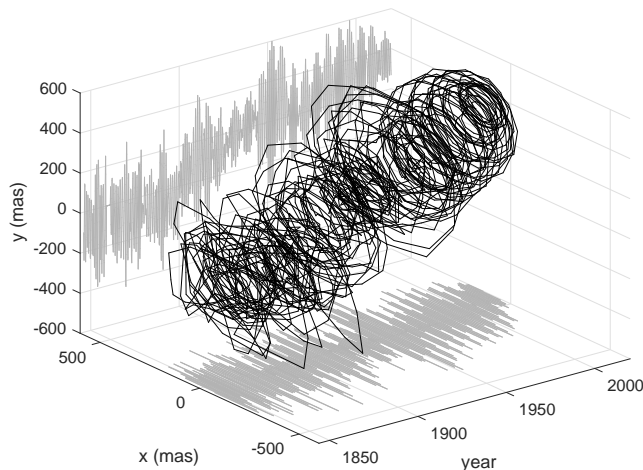


Figure 2: Earth’s polar motion from 1845 to present day, measured in regular intervals of 0.1 years.

observe a slow drift in the signal, especially in the  $y$  axis, coupled with clear oscillatory motion. We are motivated to study this dataset in particular because Arató et al. (1962) also studied Earth’s polar motion when proposing the regular proper complex OU process. Here we can make use of over 50 years’ worth of new data to provide updated parameter estimates, and test for the presence of ellipticity, using our improper SDE of (1).

In the left panel of Fig. 3 we plot the periodogram of the complex-valued signal  $z(t) = x(t) + iy(t)$ . For complex-valued signals, the periodogram is in general asymmetric over positive and negative frequencies, as directions of spin are separated in complex-valued signal modelling. Negative frequencies correspond to clockwise oscillations and positive frequencies correspond to anti-clockwise oscillations. In Fig. 3 we detect three clear peaks in the signal. The largest at frequency zero is due to the drift. The smallest, at (negative) one cycle per year, is the annual oscillation. The third, at approximately  $-0.84$  cycles per year is the Chandler wobble, discovered by astronomer Seth Carlo Chandler in 1891.

We will study the properties of both oscillations using the widely linear complex OU of (1). To do this we cannot simply look at the precise values and locations of the peaks in the spectral density—we also need to consider frequencies in the *vicinity* of the peaks, such that we can estimate the damping parameter  $\alpha_1$  of the oscillations. We have marked in blue and red (respectively) the frequencies we will use to model the Chandler and Earth wobble oscillations respectively. Specifically, the Chandler Wobble is considered in the range  $-0.73$  to  $-0.96$  cycles per year, and the annual oscillation in the range  $-0.965$  to  $-1.035$  cycles per year. We have also marked the corresponding positive frequencies, which will contain some elevated power if this component of the signal has elliptical structure.

We now bandpass filter the negative blue frequencies in the left panel of Fig. 3 corresponding to the Chandler wobble, and plot these in blue on the complex plane in the right panel of Fig. 3. We overlay the full polar motion signal in black. As we have only filtered the negative frequencies, then the oscillations appear entirely circular. We display the same filtered signal on a 3-D plot in the left panel of Fig. 4, where the varying amplitude of the signal can be clearly seen. This suggests the presence of damping in the oscillation, which motivated the construction of the regular complex OU by Arató in Arató et al. (1962). In the right panel of Fig. 4 we display the bandpassed polar motion signal over both negative and positive frequencies in blue from Fig. 3. No clear ellipticity can be observed by eye, but we will study this in more detail using the

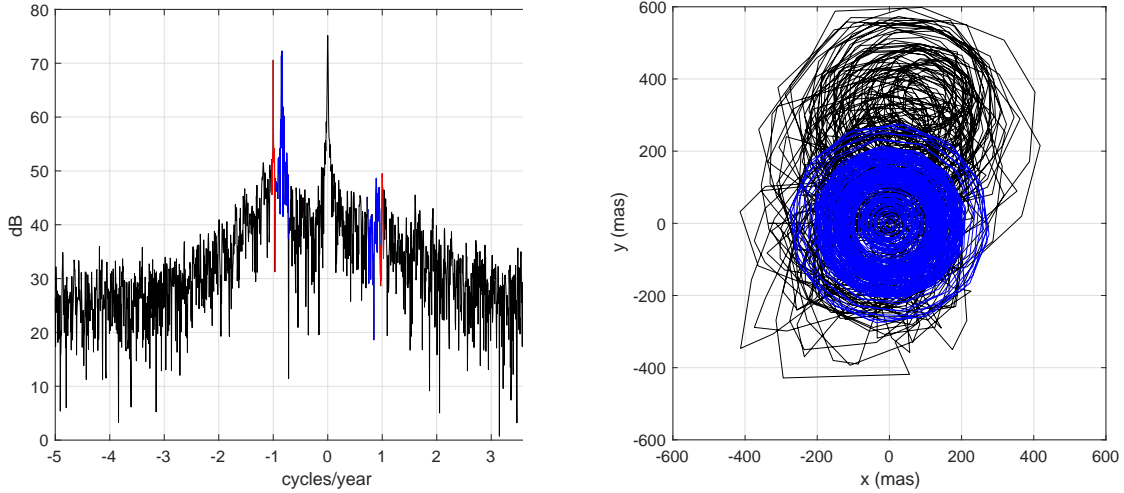


Figure 3: (Left) The periodogram of Earth’s polar motion of Fig. 2 when represented as a complex-valued signal. The red band of frequencies corresponds to the annual oscillation, and the blue band to the Chandler wobble. (Right) The Chandler wobble in the complex plane (in blue), which has been bandpass filtered from Fig. 2 using the frequencies highlighted in blue in the left panel (negative frequencies only). The full signal of Fig. 2 is plotted in black.

widely linear complex OU shortly.

First we show the bandpass filtered annual oscillations corresponding to the red frequencies in Fig. 2, over both negative and positive frequencies. These are displayed in the left and right panels of Fig. 5 in the 2-D and 3-D perspectives respectively. The ellipticity of the signal is much clearer than with the Chandler wobble in Fig. 4, and we will investigate this in more detail using the widely linear complex OU process.

We now fit complex OU processes to the data. First, we consider the Chandler Wobble over negative frequencies only and fit the regular complex OU of Arató (Arató et al., 1962), which corresponds to the widely linear complex OU (1) when  $\alpha_2 = \beta_2 = r = 0$ . We fit the parameters using the semi-parametric Whittle procedure described in Section 3. The fit of the power spectral density of the regular complex OU in (10) to the periodogram is displayed in Fig. 6. Although the periodogram is variable, it lies within the 95% confidence intervals of the modelled power spectral density almost everywhere. Confidence intervals are estimated using the asymptotic chi-squared distribution of the periodogram. The estimated parameters (to 3 significant figures) are  $\alpha_1 = 0.0425$  (in units of  $\text{years}^{-1}$ ),  $\beta_1 = -0.842$  (cycles per year) and  $\sigma^2 = 204$ .

Arató et al. (1962), in his 1962 analysis, found  $\alpha_1 = 0.09$  and  $\beta_1 = -0.839$ , but the 95% confidence range for  $\alpha_1$  was found to be  $[0.01, 0.1]$  which is consistent with our estimate. So our estimates, which utilise over 50 years of new data, are in broad agreement with Arató but we find a slightly lower damping parameter. We note however that information about the damping parameter lies over very few frequencies, and is therefore a challenging parameter to estimate. This observation was also made by Arató et al. (1962) (hence the wide confidence intervals). In other literature, Brillinger (1973) also uses a regular complex OU process like Arató, but makes some seasonal corrections, and finds  $\alpha_1 = 0.06$  cycles per year with a 95% confidence range of  $[0.006, 0.114]$ . More broadly, there still remains an active research debate on the rate of damping of the Chandler wobble (Vondrák et al., 2017), where a variety of geophysical models have been employed to measure this, but a more detailed comparison with this literature is beyond the scope of this

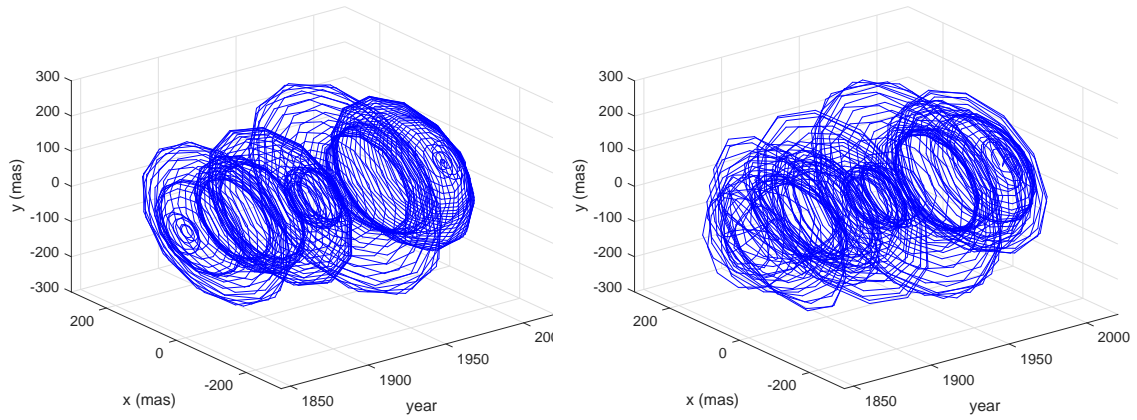


Figure 4: The Chandler wobble over time, which has been bandpass filtered from Fig. 2 using the frequencies highlighted in Fig. 3. The left panel uses negative frequencies only and the right panel uses both positive and negative frequencies.

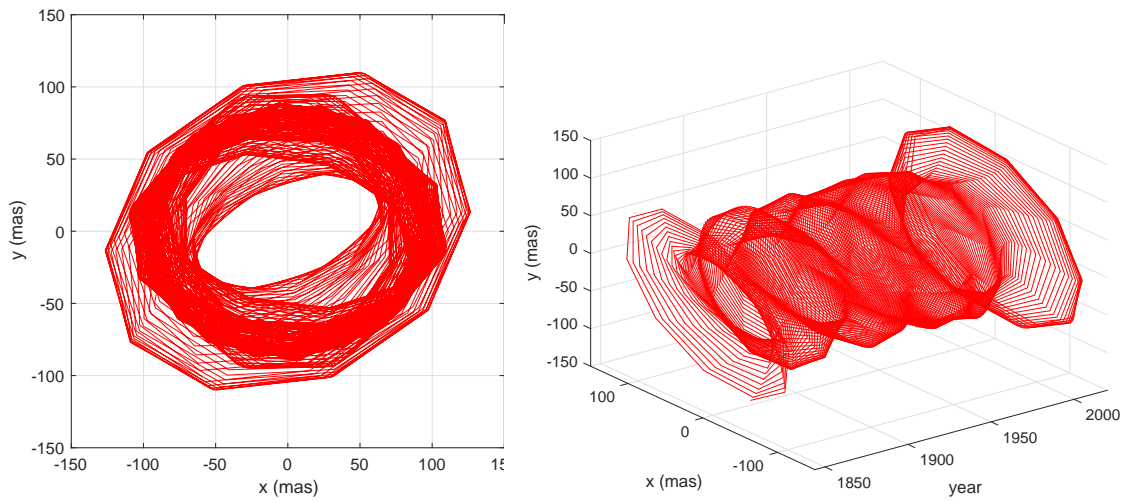


Figure 5: The annual oscillation which has been bandpass filtered from Fig. 2 using the frequencies highlighted in Fig. 3 (using both positive and negative frequencies). The left panel displays the signal in the complex plane, the right panel shows the evolution of the signal over time.

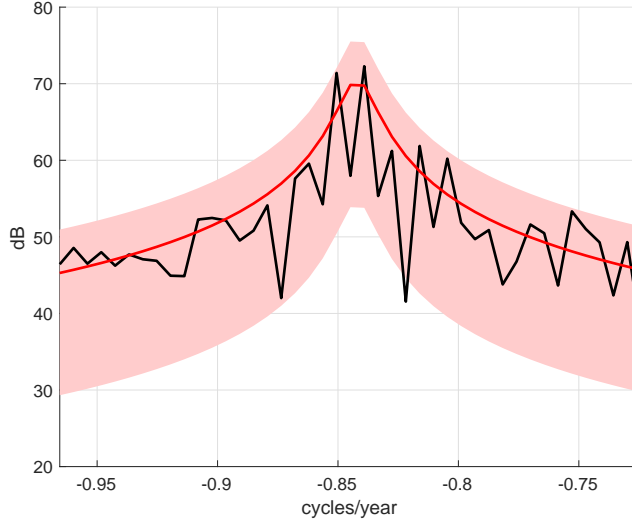


Figure 6: The fit of the power spectral density of the circular complex OU process (red) to the periodogram of Earth’s polar motion (black). The fit is performed semi-parametrically using the Whittle likelihood in the frequency interval of -0.96 to -0.73 cycles per year which captures the Chandler wobble. 95% confidence intervals of the power spectral density are in red shading.

paper.

Now we fit the widely linear complex OU to the Chandler wobble over negative and positive frequencies. We again use the semi-parametric Whittle procedure. The fits are displayed in Fig. 7. Clearly the fit to positive frequencies is poor, with no clear peak in the periodogram, and several values lying outside of the 95% confidence range at several frequencies near the peak. This is consistent with the literature where the Chandler wobble motion has been described as “*quasi-circular*” with a low eccentricity in the range  $[0.1, 0.23]$  in Höpfner (2003). The periodogram of the signal is too variable and is contaminated by other artefacts at positive frequencies, so our model is unable to detect this low eccentricity in the Chandler wobble oscillation for this reason.

We now fit the widely linear complex OU to the annual oscillation over negative and positive frequencies. The spectra are displayed in Fig. 8, and this time the model is a much better fit, even though the range of frequencies over which the fit can be performed is relatively narrow. The periodogram comfortably lies within the 95% confidence interval bands at all modelled frequencies. The estimated parameters (to 3 significant figures) are  $\{\alpha = 0.0193, \beta = -1.00, \rho = 0.793, \psi = 0.122, A^2 = 21.0\}$  in the bivariate representation of (5) and  $\{\alpha_1 = 0.0193, \beta_1 = -1.11, \alpha_2 = 0.116, \beta_2 = 0.476, \sigma^2 = 23.3, r = 9.82 + i2.44\}$  in the widely linear complex OU representation of (1). As discussed in Section 3, the orientation parameter  $\psi$  is estimated non-parametrically using (15). The eccentricity of the annual oscillation is estimated to be  $\varepsilon = \sqrt{1 - \rho^4} = 0.777$ . This is in broad agreement but slightly different from Höpfner (2003) who discover a “significantly elliptic annual motion” in the range  $[0.26, 0.49]$ . For comparison, a simple non-parametric estimate from the data from Fig. 2 using (see Sykulski et al. (2016a))

$$\hat{\varepsilon} = \frac{2\sqrt{|J_Z(\omega = 1)J_Z(\omega = -1)|}}{|J_Z(\omega = 1)| + |J_Z(\omega = -1)|},$$

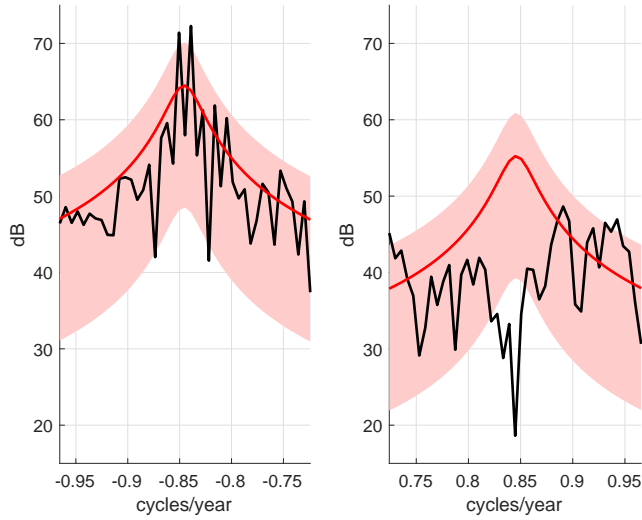


Figure 7: The fit of the power spectral density of the widely linear complex OU process (red) to the periodogram of Earth's polar motion (black). The fit is performed semi-parametrically using the Whittle likelihood in the frequency intervals of  $-0.96$  to  $-0.73$  and  $0.73$  to  $0.96$  cycles per year, which captures the (elliptical) Chandler wobble. 95% confidence intervals of the power spectral density are in red shading.

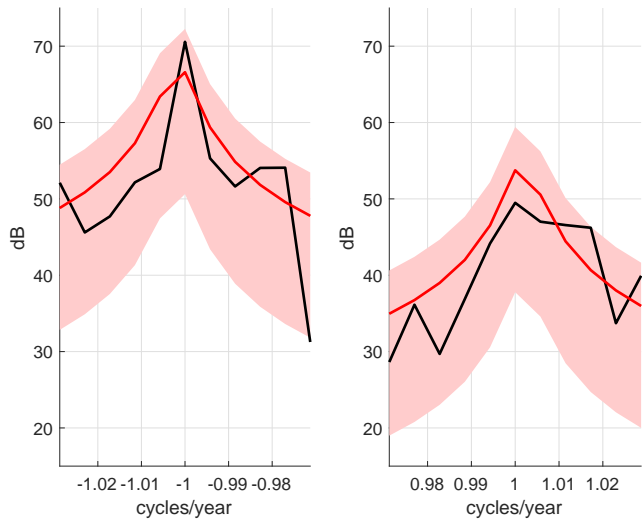


Figure 8: The fit of the power spectral density of the widely linear complex OU process (red) to the periodogram of Earth's polar motion (black). The fit is performed semi-parametrically using the Whittle likelihood in the frequency intervals of  $-1.035$  to  $-0.965$  and  $0.965$  to  $1.035$  cycles per year, which captures the (elliptical) annual oscillation. 95% confidence intervals of the power spectral density are in red shading.

yields  $\hat{\epsilon} = 0.546$ . The higher values of eccentricity we estimate as compared with Höpfner (2003) are likely due to their approach of time-windowing into small intervals, versus our approach of considering the entire signal as a stochastic process. Again, a more detailed analysis is beyond the scope of this paper, however our example here serves as a simple proof-of-concept of the potential applications of our novel continuous-time improper SDE model.

## 5 Discussion and Conclusion

Oscillations are key features of natural and human-made phenomena. Often we observe linked oscillations that map out the same periodic phenomenon. For deterministic phenomena, such have been studied in Lilly and Olhede (2009, 2011); Olhede (2013), and for stochastic phenomena in Sykulski et al. (2016a,b). Continuous time signals that are improper are, as we have shown, challenging to describe but possess interpretable multidimensional dynamics (Lilly and Olhede, 2011). The aim of this paper has been to introduce a structured form of multivariate dependence so that stochastic elliptical trajectories are mapped out, just like single oscillations can be conceptualised as mapping out circles. Complex-valued models, such as the widely linear complex OU, provide rich structural information as we can recover the geometric features of the ellipse directly from the observations and estimated parameters.

Multivariate stochastic processes have been the focus of intensive research in the last decade (Barigozzi et al., 2018; Chang et al., 2018; Che et al., 2018; Hallac et al., 2017; Nieto et al., 2016). There is much advantage to modelling underlying geometry in signals (Olhede and Walden, 2005), but that viewpoint exactly corresponds as to how the underlying structure in the observations evolves over time. Oscillations are natural as a modelling starting point when studying stationary phenomena. The multivariate generalisation of an oscillation is an observed trajectory from an ellipse (Lilly and Olhede, 2011). This puts an emphasis on the classes of models starting from oscillations, broadening to partially observed trajectories on the ellipse.

A number of questions remain unresolved. Our generalisation of the OU model is just one example of a statistical model of temporal structure. The differential equation linkage has been discussed further for other applications including random fields by Lindgren et al. (2011). We envision that similar extensions could be done to their model classes. This would build on the non-parametric statistical work of Walden (2013). Furthermore, we can seek similar extensions to trivariate and multivariate temporal signals, building stochastic analogues to the deterministic approaches taken in Lilly and Olhede (2011).

Finally our understanding of the widely linear complex OU has been significantly enhanced by the analysis of polar motion and the Chandler wobble. Polar motion data has been collected from more planets than Earth and our understanding of the model would be significantly enhanced by analysing such data and testing our model on real data structures such as Mars (Van Hoolst et al., 2000), especially as richer datasets become available from future missions making such analysis more feasible. The challenges of real data examples will stress test our model, and show us what new features and geometrical structures require incorporating into the model framework.

## Appendix A: Relationship between the OU and AR(1) Processes

Consider the widely linear complex autoregressive process of Sykulski et al. (2016a) given by

$$Z(t) = \lambda e^{i\zeta} Z(t-1) + \gamma e^{i\phi} Z^*(t-1) + \epsilon_t, \quad (16)$$

with noise variance  $\sigma_{AR}^2$  and pseudo-variance  $r_{AR}$ . Let us now contrast this with the widely linear complex OU of (1). In the simple (proper) case of  $\gamma = \alpha_2 = \beta_2 = r = r_{AR} = 0$  then a regular sampled complex

OU (at intervals  $\Delta$ ) is like a complex AR(1) where

$$\lambda = e^{-\alpha_1 \Delta}, \quad (17)$$

and

$$\sigma_{AR}^2 = \sigma^2 \frac{(1 - e^{-2\alpha_1 \Delta})}{2\alpha_1}, \quad (18)$$

and

$$\zeta = \beta_1, \quad (19)$$

thus providing a simple mapping between the processes. These relationships can be derived by considering an Euler-Maruyama expansion of the OU:

$$z(t + 1/x) \approx (1 - \alpha_1/x + i\beta_1/x)z(t) + \sqrt{A^2/x}B,$$

where  $x$  is large and  $B$  is a draw from a  $\mathcal{N}(0, 1)$  such that repeating  $x\Delta$  times we have

$$z(t + \Delta)(1 - \alpha_1/x + i\beta_1/x)^{x\Delta} z(t) + \sqrt{A^2/x} \sum_{k=0}^{x\Delta-1} (1 - \alpha_1/x)^k B,$$

and then taking  $x \rightarrow \infty$  we get the relationships above.

In the general case  $\gamma \neq \alpha_2 \neq \beta_2 \neq r \neq r_{AR} \neq 0$  then the Euler-Maruyama expansion becomes

$$z\left(t + \frac{1}{x}\right) \approx \left(1 - \frac{\alpha_1}{x} + \frac{i\beta_1}{x}\right) z(t) - \left(\frac{\alpha_2}{x} - \frac{i\beta_2}{x}\right) z^*(t) + \sqrt{\frac{1}{x}} B,$$

where  $B$  is a draw from  $\mathcal{CN}(0, \sigma^2, r)$ . Then repeating  $x\Delta$  times and taking  $x \rightarrow \infty$  we observe that

$$\lambda e^{i\zeta} = \lim_{x \rightarrow \infty} \sum_{k=0}^{x\Delta/2} \left(1 - \frac{\alpha_1}{x} + \frac{i\beta_1}{x}\right)^{x\Delta-2k} \left(\frac{\alpha_2}{x} - \frac{i\beta_2}{x}\right)^{2k} \binom{x\Delta}{2k},$$

and

$$\gamma e^{i\phi} = \lim_{x \rightarrow \infty} \sum_{j=1}^{x\Delta/2} \left(1 - \frac{\alpha_1}{x} + \frac{i\beta_1}{x}\right)^{x\Delta-2j+1} \left(\frac{\alpha_2}{x} - \frac{i\beta_2}{x}\right)^{2j-1} \binom{x\Delta}{2j-1},$$

which have no clear analytical solutions, such that we can observe the nontrivial mapping between the processes in the widely linear case.

## Appendix B: Power spectral density derivation

To derive the power spectral density of the widely linear complex OU, we start from the power spectral density of the regular complex OU in (10) and convert to Cartesian forms using the relationships given in Sykulski et al. (2017)

$$\begin{aligned} S_{\tilde{x}}(\omega) &= \frac{1}{4}\{S_{\tilde{z}}(\omega) + S_{\tilde{z}}(-\omega)\} + \frac{1}{2}\mathcal{R}\{R_{\tilde{z}}(\omega)\}, \\ S_{\tilde{y}}(\omega) &= \frac{1}{4}\{S_{\tilde{z}}(\omega) + S_{\tilde{z}}(-\omega)\} - \frac{1}{2}\mathcal{R}\{R_{\tilde{z}}(\omega)\}, \\ S_{\tilde{x}\tilde{y}}(\omega) &= \frac{1}{2}\mathcal{I}\{R_{\tilde{z}}(\omega)\} + \frac{i}{4}\{S_{\tilde{z}}(\omega) - S_{\tilde{z}}(-\omega)\}, \end{aligned}$$

where  $S_{\tilde{x}\tilde{y}}(\omega)$  is the cross-spectral density between  $\tilde{x}(t)$  and  $\tilde{y}(t)$ , and  $\mathcal{R}\{\cdot\}$  and  $\mathcal{I}\{\cdot\}$  denote the real and imaginary part respectively. Substituting in (10), and using that  $R_{\tilde{z}}(\omega) = 0$  as the regular complex OU is a proper process, we obtain

$$S_{\tilde{x}}(\omega) = \frac{A^2}{4} \left\{ \frac{1}{\alpha^2 + (\omega - \beta)^2} + \frac{1}{\alpha^2 + (\omega + \beta)^2} \right\}, \quad (20)$$

$$S_{\tilde{y}}(\omega) = \frac{A^2}{4} \left\{ \frac{1}{\alpha^2 + (\omega - \beta)^2} + \frac{1}{\alpha^2 + (\omega + \beta)^2} \right\}, \quad (21)$$

$$S_{\tilde{x}\tilde{y}}(\omega) = \frac{iA^2}{4} \left\{ \frac{1}{\alpha^2 + (\omega - \beta)^2} - \frac{1}{\alpha^2 + (\omega + \beta)^2} \right\}. \quad (22)$$

Note that  $S_{\tilde{x}}(\omega) = S_{\tilde{y}}(\omega)$ . Next we find the power spectral densities of the elliptically transformed bivariate OU process of (6). First we note by expanding (5) that

$$\begin{aligned} x(t) &= \frac{1}{\rho} \tilde{x}(t) \cos \psi - \rho \tilde{y}(t) \sin \psi, \\ y(t) &= \rho \tilde{y}(t) \cos \psi + \frac{1}{\rho} \tilde{x}(t) \sin \psi. \end{aligned}$$

This clarifies the geometric interpretation of  $P$  and  $Q$  in (5).

It then follows that

$$S_x(\omega) = \frac{\cos^2 \psi}{\rho^2} S_{\tilde{x}}(\omega) + \rho^2 \sin^2 \psi S_{\tilde{y}}(\omega) - \cos \psi \sin \psi S_{\tilde{x}\tilde{y}}(\omega) - \cos \psi \sin \psi S_{\tilde{x}\tilde{y}}^*(\omega), \quad (23)$$

$$S_y(\omega) = \frac{\sin^2 \psi}{\rho^2} S_{\tilde{y}}(\omega) + \rho^2 \cos^2 \psi S_{\tilde{x}}(\omega) + \cos \psi \sin \psi S_{\tilde{x}\tilde{y}}(\omega) + \cos \psi \sin \psi S_{\tilde{x}\tilde{y}}^*(\omega), \quad (24)$$

$$S_{xy}(\omega) = \frac{\cos \psi \sin \psi}{\rho^2} S_{\tilde{x}}(\omega) - \rho^2 \cos \psi \sin \psi S_{\tilde{y}}(\omega) + \cos^2 \psi S_{\tilde{x}\tilde{y}}(\omega) - \sin^2 \psi S_{\tilde{x}\tilde{y}}^*(\omega), \quad (25)$$

where we have used that  $S_{\tilde{y}\tilde{x}}(\omega) = S_{\tilde{x}\tilde{y}}^*(\omega)$ . Substituting (20)–(22) into (23)–(25) we obtain

$$S_x(\omega) = \frac{A^2}{4} \left( \frac{\cos^2 \psi}{\rho^2} + \rho^2 \sin^2 \psi \right) \left\{ \frac{1}{\alpha^2 + (\omega - \beta)^2} + \frac{1}{\alpha^2 + (\omega + \beta)^2} \right\}, \quad (26)$$

$$S_y(\omega) = \frac{A^2}{4} \left( \frac{\sin^2 \psi}{\rho^2} + \rho^2 \cos^2 \psi \right) \left\{ \frac{1}{\alpha^2 + (\omega - \beta)^2} + \frac{1}{\alpha^2 + (\omega + \beta)^2} \right\}, \quad (27)$$

$$\begin{aligned} S_{xy}(\omega) &= \frac{A^2}{4} \left( \frac{\cos \psi \sin \psi}{\rho^2} - \rho^2 \cos \psi \sin \psi \right) \left\{ \frac{1}{\alpha^2 + (\omega - \beta)^2} + \frac{1}{\alpha^2 + (\omega + \beta)^2} \right\} \\ &\quad + \frac{iA^2}{4} \left\{ \frac{1}{\alpha^2 + (\omega - \beta)^2} - \frac{1}{\alpha^2 + (\omega + \beta)^2} \right\}. \end{aligned} \quad (28)$$

We then convert back to complex using the relationships given in Sykulski et al. (2017)

$$S_z(\omega) = S_x(\omega) + S_y(\omega) + 2\mathcal{I}\{S_{xy}(\omega)\}, \quad (29)$$

$$R_z(\omega) = S_x(\omega) - S_y(\omega) + 2i\mathcal{R}\{S_{xy}(\omega)\}. \quad (30)$$

Substituting (26)–(28) into (29)–(30) we obtain

$$\begin{aligned}
S_z(\omega) &= \frac{A^2}{4} \left( \frac{1}{\rho^2} + \rho^2 \right) \left\{ \frac{1}{\alpha^2 + (\omega - \beta)^2} + \frac{1}{\alpha^2 + (\omega + \beta)^2} \right\} \\
&\quad + \frac{A^2}{2} \left\{ \frac{1}{\alpha^2 + (\omega - \beta)^2} - \frac{1}{\alpha^2 + (\omega + \beta)^2} \right\}, \\
R_z(\omega) &= \frac{A^2}{4} \left( \frac{1}{\rho^2} - \rho^2 \right) (\cos^2 \psi - \sin^2 \psi) \left\{ \frac{1}{\alpha^2 + (\omega - \beta)^2} + \frac{1}{\alpha^2 + (\omega + \beta)^2} \right\} \\
&\quad + \frac{iA^2}{2} \left( \frac{1}{\rho^2} - \rho^2 \right) \cos \psi \sin \psi \left\{ \frac{1}{\alpha^2 + (\omega - \beta)^2} - \frac{1}{\alpha^2 + (\omega + \beta)^2} \right\},
\end{aligned}$$

which simplify to the forms given in (11) and (12).

## References

- M. Arató, A. N. Kolmogorov, and Y. G. Sinai. Evaluation of the parameters of a complex stationary Gauss-Markov process. *Doklady Akademii Nauk SSSR*, 146:747–750, 1962.
- M. Barigozzi, H. Cho, and P. Fryzlewicz. Simultaneous multiple change-point and factor analysis for high-dimensional time series. *Journal of Econometrics*, 206(1):187–225, 2018.
- Y. Barkin and J. Ferrandiz. Elliptical Chandler pole motions of the Earth and Mars. In *EGU General Assembly Conference Abstracts*, volume 12, page 2936, 2010.
- D. R. Brillinger. An empirical investigation of the Chandler wobble and two proposed excitation processes. *Bulletin of the International Statistical Institute*, 45(3):413–434, 1973.
- P. Brockwell. Continuous-time ARMA processes. *Handbook of statistics*, 19:249–276, 2001.
- W. Brown and R. Crane. Conjugate linear filtering. *IEEE Transactions on Information Theory*, 15(4):462–465, 1969.
- J. Chang, B. Guo, Q. Yao, et al. Principal component analysis for second-order stationary vector time series. *The Annals of Statistics*, 46(5):2094–2124, 2018.
- Z. Che, S. Purushotham, K. Cho, D. Sontag, and Y. Liu. Recurrent neural networks for multivariate time series with missing values. *Scientific reports*, 8(1):6085, 2018.
- D. Hallac, S. Vare, S. Boyd, and J. Leskovec. Toeplitz inverse covariance-based clustering of multivariate time series data. In *Proceedings of the 23rd ACM SIGKDD International Conference on Knowledge Discovery and Data Mining*, pages 215–223. ACM, 2017.
- J. Höpfner. Chandler and annual wobbles based on space-geodetic measurements. *Journal of Geodynamics*, 36(3):369–381, 2003.
- B. Jelfs, D. P. Mandic, and S. C. Douglas. An adaptive approach for the identification of improper complex signals. *Signal processing*, 92(2):335–344, 2012.
- H. Kantz and T. Schreiber. *Nonlinear time series analysis*, volume 7. Cambridge university press, 2004.

- J. Lilly and J.-C. Gascard. Wavelet ridge diagnosis of time-varying elliptical signals with application to an oceanic eddy. *Nonlinear Processes in Geophysics*, 13(5):467–483, 2006.
- J. M. Lilly and S. C. Olhede. Bivariate instantaneous frequency and bandwidth. *IEEE Transactions on Signal Processing*, 58(2):591–603, 2009.
- J. M. Lilly and S. C. Olhede. Analysis of modulated multivariate oscillations. *IEEE Transactions on Signal Processing*, 60(2):600–612, 2011.
- I. V. Lindell. *Methods for electromagnetic field analysis*. Oxford University Press, Oxford, UK, 1992.
- F. Lindgren, H. Rue, and J. Lindström. An explicit link between Gaussian fields and Gaussian Markov random fields: the stochastic partial differential equation approach. *Journal of the Royal Statistical Society: Series B (Statistical Methodology)*, 73(4):423–498, 2011.
- Y. Matsuda and Y. Yajima. Fourier analysis of irregularly spaced data on  $\mathbb{R}^d$ . *Journal of the Royal Statistical Society: Series B (Statistical Methodology)*, 71(1):191–217, 2009.
- J. Navarro-Moreno. ARMA prediction of widely linear systems by using the innovations algorithm. *IEEE Transactions on Signal Processing*, 56(7):3061–3068, 2008.
- F. H. Nieto, D. Pena, and D. Saboyá. Common seasonality in multivariate time series. *Statistica Sinica*, 26(4):1389–1410, 2016.
- S. C. Olhede. Modulated oscillations in many dimensions. *Philosophical Transactions of the Royal Society A: Mathematical, Physical and Engineering Sciences*, 371(1984):20110551, 2013.
- S. C. Olhede and A. T. Walden. Local directional denoising. *IEEE Transactions on Signal Processing*, 53(12):4725–4730, 2005.
- A. Oya, J. Navarro-Moreno, and J. C. Ruiz-Molina. Widely linear simulation of continuous-time complex-valued random signals. *IEEE Signal Processing Letters*, 18(9):513–516, 2011.
- B. Picinbono and P. Bondon. Second-order statistics of complex signals. *IEEE Transactions on Signal Processing*, 45(2):411–420, 1997.
- B. Picinbono and P. Chevalier. Widely linear estimation with complex data. *IEEE Transactions on Signal Processing*, 43(8):2030–2033, 1995.
- P. M. Robinson et al. Gaussian semiparametric estimation of long range dependence. *The Annals of statistics*, 23(5):1630–1661, 1995.
- P. J. Schreier. Polarization ellipse analysis of nonstationary random signals. *IEEE Transactions on Signal Processing*, 56(9):4330–4339, 2008.
- P. J. Schreier and L. L. Scharf. Second-order analysis of improper complex random vectors and processes. *IEEE Transactions on Signal Processing*, 51(3):714–725, 2003.
- P. J. Schreier and L. L. Scharf. *Statistical signal processing of complex-valued data: the theory of improper and noncircular signals*. Cambridge University Press, 2010.

- A. M. Sykulski and D. B. Percival. Exact simulation of noncircular or improper complex-valued stationary Gaussian processes using circulant embedding. In *2016 IEEE 26th International Workshop on Machine Learning for Signal Processing (MLSP)*, pages 1–6. IEEE, 2016.
- A. M. Sykulski, S. C. Olhede, and J. M. Lilly. A widely linear complex autoregressive process of order one. *IEEE Transactions on Signal Processing*, 64(23):6200–6210, 2016a.
- A. M. Sykulski, S. C. Olhede, J. M. Lilly, and E. Danioux. Lagrangian time series models for ocean surface drifter trajectories. *Journal of the Royal Statistical Society: Series C (Applied Statistics)*, 65(1):29–50, 2016b.
- A. M. Sykulski, S. C. Olhede, J. M. Lilly, and J. J. Early. Frequency-domain stochastic modeling of stationary bivariate or complex-valued signals. *IEEE Transactions on Signal Processing*, 65(12):3136–3151, 2017.
- A. M. Sykulski, S. C. Olhede, A. P. Guillaumin, J. M. Lilly, and J. J. Early. The debiased Whittle likelihood. *Biometrika*, 106(2):251–266, 2019.
- T. Van Hoolst, V. Dehant, and P. Defraigne. Chandler wobble and free core nutation for Mars. *Planetary and Space Science*, 48(12-14):1145–1151, 2000.
- P. Vatiwutipong and N. Phewchean. Alternative way to derive the distribution of the multivariate Ornstein–Uhlenbeck process. *Advances in Difference Equations*, 2019(1):1–7, 2019.
- M. Veneziani, A. Griffa, A. M. Reynolds, and A. J. Mariano. Oceanic turbulence and stochastic models from subsurface Lagrangian data for the Northwest Atlantic Ocean. *Journal of Physical Oceanography*, 34(8):1884–1906, 2004.
- J. Vondrák, C. Ron, and Y. Chapanov. New determination of period and quality factor of Chandler wobble, considering geophysical excitations. *Advances in Space Research*, 59(5):1395–1407, 2017.
- A. Walden. Rotary components, random ellipses and polarization: A statistical perspective. *Philosophical Transactions of the Royal Society A: Mathematical, Physical and Engineering Sciences*, 371(1984):20110554, 2013.
- Y. C. Yoon and H. Leib. Maximizing SNR in improper complex noise and applications to CDMA. *IEEE Communications Letters*, 1(1):5–8, 1997.